Geomorphology
August 2013, Volume 195, Pages 45–52
http://dx.doi.org/10.1016/j.geomorph.2013.04.025

Quaternary evolution of a large alluvial fan in a periglacial setting (Crau Plain, SE France) constrained by terrestrial cosmogenic nuclide (^{10}Be)

Stéphane Molliex[1,] *, Lionel L. Siame, Didier L. Bourlès, Olivier Bellier, Régis Braucher, Georges Clauzon[2]

Aix-Marseille Université, CNRS-IRD-Collège de France, UM 34 CEREGE, BP 80, 13545 Aix-en-Provence Cedex 4, France

[1] Present address : Laboratoire Environnements Sédimentaires, Géosciences Marines, IFREMER, BP70, 29280 Plouzané, France.

[2] While this paper was being considered for publication, Georges Clauzon passed away, and we would like to dedicate this article to his memory.

*: Corresponding author : Stéphane Molliex, tel.: + 33 298224951; fax: + 33 298224570 ;
email address : smolliex@gmail.com

Abstract:

Located in the foreland of the Western Alps, the Crau Plain was the outlet of the Durance River in the Pleistocene. In order to constrain its geodynamic evolution in terms of chronology and denudation rates, the two main Quaternary deposits of this plain have been studied based on cosmogenic nuclide ^{10}Be concentration measurements along depth profiles. The abandonment of the Miramas and Luquier alluvial surfaces occurred at the beginning of glacial periods, Würm (isotopic stage 4) and Riss (isotopic stage 6), respectively. Discrepancy in denudation rates under similar geomorphological and lithological conditions suggests different denudation processes during glacial and interglacial periods. The denudation rate has been estimated at about 25 mm ka^{-1} for the interglacial period and about 60 mm ka^{-1} for the glacial period. The abandonment of the Crau Plain as the outlet of the Durance River occurred sometime between 75 and 35 ka.

Keywords: Quaternary ; Denudation rate ; Cosmic ray exposure (CRE) dating ; 10Be depth profile ; Provence ; Periglacial setting

1. Introduction

The evolution and the development of alluvial systems (terraces and fans) reflect their responses to variations in forcing factors such as climate and tectonics (e.g., Twidale, 2004). Glacio-fluvial terraces formed by erosion and/or deposition, alluvial fans and hydrographic networks are geomorphic markers that can be dated for paleoclimatic reconstructions or deciphering tectonic processes, especially on relatively short timescales (10 ka to 1 Ma; e.g. Burbank and Anderson, 2001 and Anderson and Anderson, 2010). To date Quaternary deposits, several methods have been developed in recent decades. Among them, the use of terrestrial cosmogenic nuclides has proven effective for dating geomorphological markers associated with alluvial deposits and characterizing morpho-dynamics based on long-term denudation and/or uplift rates (e.g. Brown et al., 1995; Granger et al., 1996; Kirschner et al., 2001; Schaller et al., 2001; Gosse and Philips, 2001; von Blanckenburg, 2006; Dunai, 2010; Siame et al. 2011). Although long-term denudation rates are generally of the same order of magnitude for similar environments in the European continent (Schaller et al., 2001), their impacts during different glacial and interglacial climatic conditions are often difficult to compare. In this paper, we aim at establishing such a comparison by measuring in situ-produced ^{10}Be concentrations along vertical profiles sampled within two alluvial deposits in a periglacial climatic setting with similar lithological, geomorphological, and tectonic characteristics but different ages.

For such a purpose, deposits in the Crau Plain appear well suited because of (i) abundant datable quartzite pebbles in the alluvial material; (ii) a large horizontal extent of the deposits allowing sampling away from the edges of terraces; (iii) absence of topographic barriers enabling the scaling of production rates based only on the latitude and altitude; and (iv) two distinct sets of alluvial deposits, namely the Luquier and Miramas terraces, with similar lithology and geomorphological characteristics. In the periglacial setting of the Mediterranean Provence, this study helps (i) establishes the chronology of sedimentary events in the Crau Plain, including the timing of the last Durance River diversion that likely has a tectonic origin (Molliex, 2009), and (ii) quantifies and discusses the denudation rates prevailing during the distinct climatic settings that characterize their emplacement periods.

2. Geological setting

The Crau Plain is located in the Provence domain in southeastern France, a part of the Alpine foreland (Fig. 1; Peulvast et al., 1999; Champion et al., 2000; Baroux et al., 2001; Guignard et al., 2005; Cushing et al., 2008; Molliex et al., 2011), which is mainly characterized by E-trending ramp anticlines and large NNE-trending strike-slip transfer faults. The main tectonic event responsible for the setting up of these structures occurred during the so-called “Pyreneo-Provençal” late Cretaceous to Eocene orogenic phase, especially to the west of the Salon-Cavaillon fault, where the Crau Plain extends south of the Alpilles ridge (Fig. 1). In this area, the Quaternary deformation rates have been estimated to be lower than 0.1 mm yr^{-1} (Molliex et al., 2011). The Crau Plain is an almost flat surface of approximately 600 km² composed of three stacked large alluvial sheets of limestone and siliceous cobbles deposited in a braided fluvial system (Colomb and Roux, 1978, 1986). The composition of the cobbles record a typical alpine petrographic spectrum, indicating that the plain was the former outlet of the paleo-Durance River, which now flows westward to the Rhône River along the north side of the Alpilles ridge (Fig. 1; Colomb and Roux, 1978, 1986; Warner, 2012). The northern alluvial sheet is the Arles terrace; the lateral equivalent of the local Valensole II Pliocene gravels (Clauzon, 1979) and is mainly composed of alpine Jurassic and Cretaceous limestone cobbles. Endogenic and siliceous cobbles are rare within this deposit (Colomb and Roux, 1978). To the southeast, the more recent Luquier terrace (Fx in Fig. 1) is composed of cobbles presenting a typical Quaternary alpine petrographic spectrum, represented by a mix of alpine Jurassic and Cretaceous limestone and numerous siliceous cobbles mainly of crystalline rocks, quartzites, volcanic breccia and serpentines (Colomb and Roux, 1978). The most recent Miramas terrace is located in the southeastern part of the Crau Plain (Fy in Fig. 1) and presents almost the same petrographic spectrum as the Luquier terrace and the present-day Durance terrace. The size of cobbles slightly differs; about 20 cm for the Miramas terrace and about 20–30 cm for the Luquier terrace. Moreover, alteration of crystalline rocks is more important in the Luquier terrace than in the Miramas terrace. These two deposits have a global gray tint whereas the Arles terrace has a global yellow tint.

During the Quaternary times, the downstream course of the Durance River experienced at least two successive major diversions (Gouvernet, 1959; Colomb and Roux, 1986) (Fig. 1). During the deposition of the Arles terrace, the river was flowing in the Crau Plain through the St-Pierre-de-Vance gap (Fig. 1). During the deposition of the Luquier and Miramas terraces, the river was flowing through the Lamanon gap, east of the St-Pierre-de-Vance gap (Fig. 1). Since the deposition of the Miramas terrace, the Durance River stopped flowing through the Crau Plain and has been diverted to flow north of the Alpilles ridge (Fig. 1). Previous studies suggested a tectonic influence to explain these diversions (Gouvernet, 1959; Molliex, 2009). In addition, recent observations from this area suggest that the Salon-Cavaillon fault (Fig. 1) played a major role in this river diversion (Terrier, 1991; Molliex 2009).

3. Relative chronology of the Crau Plain deposits

The relative age of the Luquier and Miramas terraces can be interpreted from both stratigraphic and morphological perspectives. Nested within the Luquier terrace, the Miramas terrace is the youngest terrace (Colomb and Roux, 1978, 1986). This is also evidenced by the red soils, very rich in ferrous minerals, which cover the Luquier terrace, suggesting a more advanced pedogenesis. The sedimentary and structural relationships of the Quaternary deposits also help constrain their relative ages (Fig. 2). A local alluvial formation, probably deposited by a tributary of the Durance River, is stacked into the Luquier terrace but covered by the Miramas terrace (Colomb et al., 1970). This deposit, locally called the Grans terrace, contains gastropods that are characteristic of the late Riss, early Würm (isotopic stage 5e, about 125 ka; Colomb et al., 1969). The deposition of the Luquier terrace thus predates that of the Grans terrace, while the deposition of the Miramas postdates it. To the north of the Crau Plain, an alluvial fan made of cryoclastic gravel covers the oldest, post-diversion Durance terrace (Fig. 2). A snail found at the base of this fan yielded an uncalibrated ^{14}C age of 28.2 ± 0.46 ka (Evin et al., 1983). Using the calibration curve of Fairbanks et al. (2005), the calibrated age is 33.7 ± 0.5 ka. Therefore, the abandonment of the Miramas terrace occurred between 125 and 34 ka, while that of the Luquier terrace predates 125 ka (Fig. 2).

4. Methods

Cosmogenic nuclides have been widely applied to soils and bedrock outcrops to measure their duration of exposure to cosmic rays (e.g., Gosse and Phillips, 2001). Among various applications, the measurement of in-situ produced ^{10}Be concentrations along depth profiles sampled below the surface (Siame et al., 2004; Wolkowinsky and Granger, 2004) is highly useful for determining the ages of fluvial terraces (Siame et al., 2004, 2012; Braucher et al., 2009; Carcaillet et al., 2009; Hidy et al., 2010; Rixhon et al., 2011). This approach allows not only estimating ages of terrace abandonment but also denudation rates, and the inherited content of the fluvial gravels prior to their deposition (Braucher et al., 2009; Hidy et al., 2010).

From a theoretical point of view, for any sediment experiencing a single exposure history at a constant denudation rate, one can minimize the difference between the measured ^{10}Be concentrations and those predicted by the theory, using a chi-square (χ^2) procedure (Siame et al., 2004). Recently, Braucher et al. (2009) have mathematically demonstrated the uniqueness of the time–denudation solution that can be retrieved from a depth profile, and proposed a Monte Carlo procedure to generate randomly a large number of depth profiles within the analytical uncertainties of the measured cosmogenic concentrations. To establish a chronological framework for the studied deposits, we followed the procedure of Braucher et al. (2009), using measured cosmogenic ^{10}Be along relatively deep depth profiles to model the exposure time (t) and the denudation rate (ε). In order to quantify both the denudation rate and exposure duration of a given deposit, a depth profile must be deep enough to discriminate between cosmogenic nuclide concentrations mainly due to production by neutrons and those almost exclusively due to muons. The concentrations at the upper part (<3 m) of the profile, dominated by the efficiently attenuated neutrons that rapidly reach steady-state, providing an estimate of the denudation rate; whereas, the concentrations at the lower part (>3 m), dominated by the significantly less attenuated muons, provides an estimate of the exposure duration (Braucher et al., 2009). It is therefore important to sample a vertical profile as deep as possible and as far as possible from the edges of terraces. If a unique (t, ε) solution can theoretically be found (Braucher et al., 2009), the measured concentrations are never exactly fitted by the model. Indeed, the combination of both measurement errors and natural variability linked to post-depositional processes such as bioturbation, cryoturbation, and compaction results in uncertainties in the models (Granger, 2006).

In this study, we used in situ-produced ^{10}Be resulting from spallation and muonic reactions on silicon and oxygen in quartz minerals. The chemical treatment of the samples were carried out at the Laboratoire National des Nucléides Cosmogéniques (LN2C) in the Centre Européen de Recherche et d'Enseignement des Géosciences de l'Environnement (CEREGE), Aix-en-Provence, France. Samples were prepared for ^{10}Be concentration measurements following chemical procedures of Brown et al. (1991) and Merchel and Herpers (1999). After sieving (fraction comprised between 1 and 0.250 mm), samples passed through magnetic separation, and non-magnetic fraction were selectively etched in fluorosilicic and hydrochloric acids to eliminate all mineral phases but quartz. Quartz minerals then underwent a series of selective etching in hydrofluoric acid to eliminate potential surface contamination by ^{10}Be produced in the atmosphere (e.g., Brown et al., 1991). The cleaned quartz minerals were then completely dissolved in hydrofluoric acid with 100 µl of an in-house 3.10^{-3} g/g ^{9}Be carrier solution prepared from deep-mined phenakite (Merchel et al., 2008). Hydrofluoric and Perchloric fuming was used to remove fluorides and cation and anion exchange chromatography was used to eliminate iron, aluminum, manganese and other elements. Beryllium oxide was mixed to a 325-mesh niobium powder prior to measurements by Accelerator Mass Spectrometry (AMS) performed at ASTER (Aix-en-Provence) AMS French facilities. The obtained ^{10}Be/^{9}Be ratios were corrected for procedural blanks and calibrated against the National Institute of Standards and Technology standard reference material 4325 by using an assigned value of $2.79 \pm 0.03 \times 10^{-11}$ and a ^{10}Be half-life of $(1.39 \pm 0.01) \times 10^{6}$ years used as recommended by Korschinek et al. (2010) and Chmeleff et al. (2010) according to their two independent measurements. Analytical uncertainties (reported as 1σ) include uncertainties associated with AMS counting statistics, chemical blank measurements and AMS internal error (0.5%). At ASTER, long-term AMS measurements of procedural blanks yield a background ratio of $3.0 \pm 1.5 \times 10^{-15}$ for ^{10}Be/^{9}Be (Arnold et al., 2010). A sea level, high-latitude (SLHL) spallation production of 4.03±0.18 at g^{-1} yr^{-1} was used and scaled for latitude (Stone, 2000) and elevation. This production rate is a weighted mean of recently calibrated production rates in the northern hemisphere (Northeastern North America: Balco et al., 2009; Northern Norway: Fenton et al., 2011; southern Norway: Goehring et al. 2012; and Greenland: Briner et al., 2012). The contribution of muons to the production rate was calculated using the physical parameters recently re-evaluated by Braucher et al. (2011).

5. Sampling area

Two depth profiles, 15 km from each other, were sampled within the Miramas and the Luquier alluvial deposits at elevations of 46 and 17 m, respectively (Fig. 1). The Miramas profile was sampled in a gravel quarry localized between Entressen and Miramas Villages (Fig. 1). Because of soil removal in the quarry, three surface samples were also collected in a nearby, non-cultivated field. However, reconstructing the pristine elevation of the surface before soil removal is imperative to determine the exact depth position of each sample. This was performed by interpolating topographic profiles from differential GPS surveys on each sides of the quarry. The thickness of removed soil is estimated at ~35 cm, which is consistent with measured soil thicknesses near the sampling site. Ten samples of white quartzite pebbles were then collected along a vertical depth profile (30 to 480 cm in reconstituted depths; Fig. 3). The Luquier profile has been sampled along a refreshed face of an abandoned gravel quarry located in Mas Chausson (Fig. 1). Four samples were collected at the surface. The presence of a calcrete capping the surface indicates that this area has never been affected by significant human activities. Twelve samples of white quartzite pebbles were collected along a vertical depth profile (35 to 580 cm; Fig. 3).

6. Results

6.1. Surface samples

The in-situ produced ^{10}Be concentrations measured in surface samples range from 3.11×10^5 to 5.04×10^5 at g-SiO_2^{-1} for the Miramas profile, and from 2.79×10^5 to 4.31×10^5 at g-SiO_2^{-1} for the Luquier profile (Table 1). The observed scatter of surface concentrations at both sites may result from differential erosion due to the heterogeneous lithology of the pebbles constituting the studied terraces. Fig. 4 shows the inferred effects of surface processes and their consequences in the distribution of surface ^{10}Be concentrations for homogeneous and heterogeneous terrace lithologies. As limestone dissolves faster than quartzite, dissolution is not homogeneous over polygenic terraces, yielding quartzite pebble enrichments close to the surface. In addition, since the absence of topographic gradient that limits the effects of illuviation after depletion of the terrace, quartzite pebbles subjected to different exposure durations at various depths may reach the surface (Fig. 4). This model is supported by field observations indicating that erosion is mainly controlled by dissolution of carbonates combined with weathering and disintegration of crystalline clasts (chemical parameters), and illuviation of the silty matrix (physical parameters). This kind of behavior has also been described for boulders in the Himalayas (Heyman et al., 2010). These processes may explain: (i) the scatter of ^{10}Be concentrations measured on surface samples, and (ii) their relative inconsistency with the concentrations measured along the underlying depth profiles for which a constant denudation rate is modeled. The surface sample concentrations were thus not included in the modeling of ^{10}Be concentrations as a function of depth.

6.2. Depth profiles: exposure ages and denudation rates

6.2.1. Miramas terrace

Although samples M65, M160 and M210 do not perfectly match with the theoretical decay curve, the measured concentrations exhibit the expected theoretical exponential decrease (Fig. 5 and Table 1). The small difference between the measured and theoretical concentrations evidenced for samples M65 and M210 may result either from experimental uncertainties or from a sedimentary history more complex than that assumed by the model. The discrepancy observed for sample M160 suggests a more important inherited component, and therefore this sample was not included for the profile modeling. The modeled density for the terrace material is 2.1 g cm^{-3}. The inherited component deduced from the ^{10}Be concentration measured in the deepest sample is ~22 000 at/g-SiO_2 (Fig. 5a). Given these parameters, the best combination of the exposure age and the denudation rate from the modeling is 73 ka and 3.5 mm ka^{-1}, respectively. Estimates of uncertainties based on χ^2 values as proposed by Siame et al. (2004) limits the exposure age of the Miramas terrace to between 61 and 107 ka and the denudation rate between 0 and 8.5 mm ka^{-1} (Fig. 5b).

6.2.2. Luquier terrace

Although samples L305, L415 and L510 do not perfectly match with the theoretical decay curve, the measured concentrations exhibit the theoretically expected exponential decrease (Fig. 6 and Table 1). The differences between the measured and the theoretical concentrations evidenced for samples L415 and L510 may result from either experimental uncertainties or a sedimentary history more complex than assumed by the model. The more significant discrepancy observed for sample L305 might indicate a more important inherited component. Samples L355, L415 and L510 were therefore not considered for modeling. The modeled density for the terrace material is similar to that determined for the Miramas terrace, 2.1 g cm^{-3}. The inherited component deduced from the ^{10}Be concentration measured in the deepest sample is 22 000 at g-SiO_2^{-1} (Fig. 6a), similar again to that determined at the Miramas terrace, which is consistent with the observation that both deposits had the same sedimentary source. The best combination of the exposure age and denudation rate from the modeling is 181 ka and 30.9 mm ka^{-1}, respectively. Accounting for modeling uncertainties, the exposure age of the Luquier terrace is limited between 105 and 285 ka and its denudation rate between 28 and 34 mm ka^{-1} (Fig. 6b).

7. Discussion

7.1. Exposure ages

The obtained exposure ages are consistent with previous studies dealing with ages of alluvial terraces inferred from in-situ produced ^{10}Be concentrations. About 110 km upstream along the Durance River, Siame et al. (2004) suggested an age of 70 ka for one of the Manosque terraces, which can be stratigraphically correlated with the Miramas terrace. Similarly, in the same catchment, Brocard et al. (2003) proposed an age of 190 ka for a terrace of the Drac River in the Alps, which is similar to that obtained for the Luquier terrace (180 ka) implying that these two terraces can also be stratigraphically correlated. The determined ages are also consistent with the chronology inferred from paleontological constraints (Fig. 2) and the global climate model of Winograd et al. (1997) (Fig. 7). Because the abandonment of alluvial terraces is generally associated with a fall of the base level that causes stream incision, the abandonment of the Miramas terrace ca. 75 ka ago may have occurred in response to the global sea-level fall at the beginning of the Würmian glaciation (isotopic stage 4; Fig. 7). Similarly, the abandonment of the Luquier terrace at ca. 180 ka may correspond to the beginning of the Rissian cooling phase (160 to 190 ka; Fig. 7). These results also help constrain the chronology of the last diversion of the Durance River north of the Alpilles ridge, after the abandonment of the Miramas terrace (ca. 75 ka) and before the deposition of the cryoclastic fan gravel sealing the post-diversion terrace (ca. 35 ka; Fig. 2). Therefore, the last diversion of the Durance River has occurred about 55±20 ka ago. This age corresponds to the abandonment of the Crau Plain as the outlet of the Durance River.

7.2. Denudation rates

The average denudation rate for the Luquier terrace (~31 mm ka^{-1}) is consistent with the rates associated with other terraces in the same region that have been estimated using the ^{10}Be method (Brocard et al., 2003; Siame et al., 2004) or a traditional geomorphological approach (Bornand, 1978). These regional rates, ranging from 20 to 40 mm ka^{-1}, also agree with denudation rates determined in Western Europe (Schaller et al., 2001). The average denudation rate for the Miramas terrace (~3.5 mm ka^{-1}) is significantly lower, although the geomorphology and the lithology of the Miramas and Luquier terraces are similar. This discrepancy reflects exposure to different types of climate associated with glacial cycles. During the glacial periods wind erosion prevailed in the Crau Plain as shown by the high-density of dreikanters developed on the terrace surfaces (Ambert, 1988) and the formation of large-scale eolian depressions (Ambert and Clauzon, 1992); while during interglacial periods, chemical erosion with decarbonation to form fersiallitic soils has been dominant (Bonnet and Bornand, 1970; Bornand, 1978).

Before the abandonment of the Luquier terrace at the onset of the Rissian glaciation, climate was not favorable for soil development, and wind deflation was inactive because the surface was almost exclusively composed of pebbles. Therefore, the denudation rate during the Rissian glaciation was most likely very low. Conversely, during the Riss–Würm interglacial period (130–75 ka), rapid weathering occurred to form fersiallitic red soils on the Luquier terrace (Bonnet and Bornand, 1970). During the Würmian glaciation (75–15 ka), the soil developed was partly gone with the wind and quartzite cobbles concentrated at the surface. Similarly, the Miramas terrace, abandoned at the onset of the Würmian glaciation, was not initially affected by deflation due to lack of soil, and denudation was probably negligible during this period. During the Holocene, denudation by decarbonation and pedogenesis occurred as in the Riss–Würm interglacial. The resulting total thickness reduction can be computed for each terrace from the average denudation rates and associated exposure ages. For the Miramas terrace, the total thickness reduction is 26 cm (3.5 mm ka^{-1} during 75 ka), while it is about 560 cm for the Luquier terrace (31 mm ka^{-1} during 180 ka).

As discussed, the denudation rate derived from the Miramas profile is probably representative for the Holocene period. Therefore, an inferred Holocene denudation rate of 26 cm in 10 ka (26 mm ka^{-1}) can be proposed. Extrapolating this value to the interglacial intervals experienced by the Luquier terrace, that is to say, 10 ka during the Holocene and 60 ka during the Riss–Würm interglacial, yields a surface lowering of about 180 cm (Fig. 7). Because the total surface lowering estimated for this terrace is 560 cm, the remaining 380 cm should have been reduced during the Würmian glaciation, giving ~63 mm ka^{-1} as a denudation rate during the glacial period (380 cm in 60 ka). Such a high denudation rate agrees with the described large accumulations of eolian sands and dunes associated with cryoclastic gravel in Provence (Gabert, 1965). These sediments were transported and deposited by the so-called *Mistral*, a northern strong wind from the Rhône Valley. During the glacial periods, the paleo-Mistral led to a very cold local climate as indicated by markers such as cryoclastic gravels and polygonal striated soils (Arnal, 1971), distribution of landsnail species (Magnin, 1991), and multi-kilometer scale landforms due to wind erosion such as eolian depressions (Ambert and Clauzon, 1992). Wind deflation thus appears to be a significant process during glacial periods in Provence.

8. Conclusion

This study has highlighted different denudation processes affecting abandoned terraces in a temperate periglacial region, southeastern France. It has estimated the denudation rates of the studied terraces during either the Würm period dominated by wind deflation or the interglacial periods dominated by decarbonation. Although wind deflation was efficient only if soil had already developed during the preceding interglacial period, the estimated denudation rates for the glacial period are more than two times higher than those estimated for the interglacial periods. This result may explain discrepancy between the long-term denudation rates deduced from cosmogenic nuclides and those from the Holocene terraces. For polygenic terraces, therefore, not only surface samples but also deep samples along a depth profile are needed to determine the exposure age in addition to the denudation rate. This study has also provided local constraints on the abandonment age of the two alluvial terraces of the Crau Plain and allows estimating the age of the last diversion of the Durance River, flowing north of the Alpilles ridge. The estimated abandonment age of this Rissian terrace is ~190 ka, and that of the youngest terrace is ~70 ka. These chronologies are consistent with those already proposed in the literature and with the ages inferred from stratigraphic paleontology.

Acknowledgments:

While this paper was being considered for publication, Georges Clauzon passed away and we would like to dedicate this article to his memory. This study is a contribution to the CASHIMA project supervised by Fabrice Hollender (CEA). Stéphane Molliex benefited from a PhD scholarship funded by the CEA and the Conseil Regional PACA. We are grateful to the ASTER team (Maurice Arnold, Georges Aumaître, Karim Keddadouche) for the cosmogenic nuclide concentration measurements. The measurements performed at the ASTER AMS national facility (CEREGE, Aix en Provence) are supported by the INSU/CNRS, the French Ministry of Research and Higher Education, IRD and CEA. We thank Daniel Hermitte, Jules Fleury and Philippe Dussoulliez for assistance in field soil sampling and GPS measurements, Cécile Miramont for discussions, three anonymous reviewers and editor Takashi Oguchi for their fruitful comments. We are also grateful to Timothy Byrne for proof reading the manuscript. We also thank the “gravière des Jumeaux” quarry and “Mas Chausson” owners for giving authorizing us to sample.

References

Anderson, R.S., Anderson, S.P., 2010. Geomorphology: The Mechanics and Chemistry of Landscapes. Cambridge University Press, Cambridge, 640 pp.

Ambert, P., 1988. L’érosion éolienne péri-glaciaire dans le Sud-Est de la France. Géologie Alpine, mem. HS 14, 227-234.

Ambert, P., Clauzon, G., 1992. Morphogénèse éolienne en ambiance périglaciare : les dépressions fermées du pourtour du Golfe du Lion (France méditerranéenne). Zeitschrift für Geomorphologie N. F., Suppl-Bd. 84, 55-71.

Arnal, H., 1971. Phénomènes périglaciaires dans la basse valles du Rhône. Formations quaternaires du rebord sud et alluvions du fond de l’étang de Pujaut. Bulletin de l’Association française pour l’étude du Quaternaire 8 (3), 145-149.

Arnold, M., Merchel, S., Bourles, D.L., Braucher, R., Benedetti, L., Finkel, R.C., Aumaître, G., Gottdang, A., Klein, M., 2010. The French accelerator mass spectrometry facility ASTER: Improved performance and developments. Nuclear Instruments and Methods in Physics Research B 268, 1954 - 1959.

Balco, G., Briner, J., Finkel, R.C., Rayburn, J.A., Ridge, J.C., Schaefer, J.M., 2009. Regional beryllium-10 production rate calibration for late-glacial northeastern North America. Quaternary Geochronology 4, 93-107.

Baroux, E., Béthoux, N., Bellier, O., 2001. Analyses of the stress field in southeastern France from earthquake focal mechanisms. Geophysical Journal International 145, 336-348.

Bonnet, A. Bornand, M., 1970. Pédologie et Quaternaire dans la vallée du Rhône moyen. Bulletin de l’association française pour l’étude du Quaternaire. 2-3, 105-116.

Bornand, M., 1978. Altération des matériaux fluvio-glaciaires, genèse et évolution des sols sur terrasses quaternaires dans la moyenne vallée du Rhône, Thèse, Université du Languedoc. 329 pp.

Braucher, R., Del Castillo, P., Siame, L., Hidy, A.J., Bourlès, D.L., 2009. Determination of both exposure time and denudation rate from an in situ-produced 10Be depth profile: A mathematical proof of uniqueness. Model sensitivity and applications to natural cases. Quaternary Geochronology 4, 56-67.

Braucher, R., Merchel, S., Borgomano, J., Bourlès, D.L., 2011. Production of cosmogenic radionuclides at great depth : a multi element approach. Earth and Planetary Science Letters 309, 1-9.

Briner, J.P., Young, N.E., Goehring, B.M., Schaefer, J.M., 2012. Constraining Holocene ^{10}Be production rates in Greenland. Journal of Quaternary Science 27, 2-6.

Brocard, G.Y., van der Beek, P.A., Bourlès, D.L., Siame, L.L., Mugnier, J.-L., 2003. Long-term fluvial incision rates and postglacial river relaxation time in the French Western Alps from 10Be dating of alluvial terraces with assessment of inheritance, soil development and wind ablation effects. Earth and Planetary Science Letters 209, 197-214.

Brown, E.T., Edmond, J.M., Raisbeck, G.M., Yiou, F., Kurz, M.D., Brook, E.J., 1991, Examination of surface exposure ages of Antarctic moraines using in situ produced ^{10}Be and ^{26}Al: Geochimica et Cosmochimica Acta 55, 2269-2283.

Brown, E.T., Stallard, R.F., Larsen, M.C., Raisbeck, G.M., Yiou, F., 1995. Denudation rates determined from the accumulation of in situ produced ^{10}Be in the Luquillo Experimental Forest, Puerto Rico, Earth and Planetary Science Letters 129, 193–202.

Burbank, D.W., Anderson, R.S., 2001. Tectonic Geomorphology, Blackwell Science, Malden, 274 pp.

Carcaillet, J., Mugnier, J.L., Koçi, R., Jouanne, F., 2009. Uplift and active tectonics of southern Albania inferred from incision of alluvial terraces. Quaternary Research 71, 465–476.

Champion, C., Choukroune, P., Clauzon, G., 2000. La déformation post-Miocène en Provence occidentale. Geodinamica Acta 13, 67-85.

Chmeleff, J., von Blanckenburg, F., Kossert, K., Jakob, J, 2010. Determination of the ^{10}Be half-life by multicollector ICP-MS and liquid scintillation counting. Nuclear Instruments and Methods in Physics Research B 268, 192- 199.

Clauzon, G., 1979. Le canyon messinien de la Durance (Provence, France) : une preuve paléogéographique du bassin profond de dessication. Palaeogeography, Palaeoclimatology, Palaeoecology 29, 15-40.

Colomb, E., Gervais, J., Puissegur, J.-J., Roux, R.-M., 1969. Présence de niveaux a faune d'âge rissien sous le cailloutis de la Crau de Miramas. Compte-Rendude l'Académie des Sciences de Paris 268, 1683-1685.

Colomb, E., Gervais, J., Roux, R.-M., 1970. Les cailloutis quaternaires des environs de Grans (B.-du-Rh). Bulletin du muséum d'histoire naturelle de Marseille 30, 165-188.

Colomb, E., Roux, R.-M., 1978. La Crau. Données nouvelles et interprétations. Géologie méditerranéenne, V(3), 303-324.

Colomb, E., Roux, R.-M., 1986. La Crau, histoire Plio-Pléistocène. Méditerranée, 3, p. 31-42.

Cushing, E. M., Bellier, O., Nechtschein, S., Sébrier, M., Lomax, A., Volant, P., Dervin, P., Guignard, P., Bove, L., 2008. A multidisciplinary study of a slow-dipping fault for seismic hazard assessment. The exemple of the Middle Durance Fault (SE France). Geophysical Journal International 172, 1163-1178.

Dunai, T.J., 2010. Cosmogenic nuclides. Principles, Concept and Applications in the Earth Surface Sciences. Cambridge University Press, Cambridge, 187 pp.

Evin, J., Marechal, J., Marien, G., 1983. Lyon natural radiocarbon measurements IX. Radiocarbon, 25, 1, p. 59-128.

Fairbanks, R.G., Mortlock, R.G., Chiu, T.-C, Cao, L., Kaplan, A., Guilderson, T.P., Fairbanks, T.W., Bloom, A.L., Grootes, P.M., Nadeau, M.-J., 2005. Radiocarbon calibration curve spanning 0 to 50,000 Years B.P. based on paired 230Th/234U/238U and 14C dates on pristine corals. Quaternary Science Reviews 24, 1781-1796.

Fenton, C.R., Hermanns, R.L., Blikra, L.H., Kubik, P.W., Bryant, C., Niedermann, S., Meixner, A., Goethals, M.M., 2011. Regional 10Be production rate calibration for the past 12ka deduced from the radiocarbon-dated Grotlandsura and Russenes rock avalanches at 69°N, Norway. Quaternary Geochronology 6, 437-452.

Gabert, P., 1965. Phénomènes périglaciares du Qauternaire supérieur et néotectonique dans la région de l'étang de Berre (Basse-Provence occidentale). 90° congrès des sociétés savantes, tome II, p.76-88.

Goehring, B.M., Lohne, Ø.S., Mangerud, J., Svendsen, J.I., Gyllencreutz, R., Schaefer, J.M., Finkel, R.C., 2012. Late Glacial and Holocene beryllium-10 production rates for western Norway. Journal of Quaternary Science 27, 89-96.

Gosse, J.C., Phillips, F.M., 2001. Terrestrial in situ cosmogenic nuclides: Theory and application, Quaternary Science Reviews 20, 1475-1560.

Gouvernet, C., 1959. Evolution géologique des relations Bas-Rhône - Basse Durance pendant les temps pliocènes et quaternaires. Annales de la Faculté des Sciences de Marseille 29, 273-279.

Granger, D.E, Kirchner, J.W., Finkel, R., 1996. Spatially averaged long-term erosion rates measured from in situ-produced cosmogenic nuclides in alluvial sediment, Journal of Geology 104, 249–257.

Granger, D.E., 2006. A review of burial dating methods using 10Be and 26Al: in situ produced cosmogenic nuclides and quantification of geological processes. Geological Society of America Special Paper 415, 1-16.

Guignard, P., Bellier, O., Chardon, D., 2005. Géométrie et cinématique post-oligocène des failles d'Aix et de la moyenne Durance (Provence, France). Comptes Rendus Géosciences 337, 375-384.

Heyman, J., Stroeven, A.P., Harbor, J.M., Caffee, M.W., 2010. Too young or too old: Evaluating cosmogenic exposure dating based on an analysis of compiled boulder exposure ages. Earth and Planetary Science Letters 302, 71-80.

Hidy, A. J., Gosse, J.C., Pederson, J.L., Mattern, J.P., Finkel, R.C., 2010. A geologically constrained Monte Carlo approach to modeling exposure ages from profiles of cosmogenic nuclides: An example from Lees Ferry, Arizona, Geochemistry Geophysics Geosystems 11, Q0AA10, doi: 10.1029/2010GC003084.

Kirchner, J.W., Finkel, R.C., Riebe, C.S., Granger, D.E., Clayton, J.L., King, J.G., Megahan, W.F., 2001. Mountain erosion over 10 yr, 10 k.y., and 10 m.y. time scales. Geology 29, 591– 594.

Korschinek, G., Bergmaier, A., Faestermann, T., Gerstmann, U.C., Knie, K., Rugel, G.,Wallner, A., Dillmann, I., Dollinger, G., von Gostomski, Lierse Ch., Kossert, K., Maitia,M., Poutivtsev, M., Remmert, A., 2010. A new value for the half-life of 10Be by Heavy-Ion Elastic Recoil Detection and liquid scintillation counting. Nuclear Instruments and Methods in Physics Research B. 268, 187–191.

Magnin, F., 1991. Mollusques continentaux et histoire quaternaire des milieux méditerranéens (Sud-Est de la France, Catalogne). Unpublished Thesis, Université Aix-Marseille II.

Merchel, S., Herpers, U., 1999. An update on radiochemical separation techniques for the determination of long-lived radionuclides via accelerator mass spectrometry. Radiochimica Acta 84, 215-219.

Merchel S., Arnold M., Aumaitre G., Benedetti L., Bourles D.L., Braucher R., Alfimov V., Freeman S.P.H.T., Steier P., Wallner A., 2008. Towards more precise ^{10}Be and ^{36}Cl data from measurements at the 10^{-14} level: Influence of sample preparation. Nuclear Instruments and Methods in Physics Research B 266, 4921- 4926.

Molliex, S., 2009. Caractérisation de la déformation tectonique récente en Provence (SE France). PhD thesis, Aix-Marseille III University, 350 pp.

Molliex, S., Bellier, O., Terrier, M., Lamarche, J., Martelet, G., Espurt, N., 2011. Tectonic and sedimentary inheritance on the structural framework of Provence (SE France): Importance of the Salon-Cavaillon fault. Tectonophysics 501, 1-16

Peulvast, J.-P., Baroux, E., Bellier, O., Sébrier, M., 1999. Le problème de l'activité des failles de Nîmes, de Salon-Cavaillon et de la Moyenne Durance (SE France): apports de la géomorphologie structurale. Géomorphologie : relief, processus, environnement 4, 327-358.

Rixhon, G., Braucher, R., Bourlès, D., Siame, L., Bovy, B., Demoulin, A., 2011. Quaternary river incision in NE Ardennes (Belgium): Insights from 10Be/26Al dating of river terraces. Quaternary Geochronology 6, 273-284.

Schaller, M., von Blanckenburg, F., Hovius, N., Kubik, P.W., 2001. Large-scale erosion rates from in situ-produced cosmogenic nuclides in European river sediments. Earth and Planetary Science Letters 188, 441-458.

Siame, L., Bellier, O., Braucher, R., Sébrier, M., Cushing, M., Bourlès, D., Hamelin, B., Baroux, E., de Voogd, B., Raisbeck, G., Yiou, F., 2004. Local erosion rates versus active tectonics:

cosmic ray exposure modeling in Provence (SE France). Earth and Planetary Science Letters 220, 345-364.

Siame, L.L., Angelier, J., Chen, R.-F., Godard, G., Derrieux, F., Bourlès, D.L., Braucher, R., Chang, K.-J., Chu, H.-T., Lee, J.-C., 2011. Erosion rates in an active orogen (NE Taiwan): A confrontation of cosmogenic measurements with river suspended loads. Quaternary Geochronology 6, 246-260.

Siame, L.L., Chen, R.-F., Derrieux, F., Lee, J.-C., Chang, K.-J., Bourlès, D.L., Braucher, R., Léanni, Laetitia, Kang, Chu-Chun, Chang, C.-P., Chu, H.-T., 2012. Pleistocene alluvial deposits dating along frontal thrust of Changhua Fault in western Taiwan: The cosmic ray exposure point of view. Journal of Asian Earth Sciences 51, 1-20.

Stone, J.O., 2000. Air pressure and cosmogenic isotope production. Journal of Geophysical Research 105, 23753–23759.

Terrier, M., 1991. Néotectonique de la Provence occidentale (France): vers une analyse multicritère des déformations récentes. Application à la classification des structures sismogènes. PhD Thesis, Aix-Marseille 1 University, Doc. BRGM 207, 232 pp.

Twidale, C.R., 2004. River pattern and their meaning. Earth-Science Reviews 67, 159-218.

Von Blanckenburg, F., 2006. The control mechanisms of erosion and weathering at basin scale from cosmogenic nuclides in river sediment. Earth and Planetary Science Letters 242, 224-239.

Warner, R.F., 2012. A Morphological Study of Durance River Terraces from Tallard to Avignon, South-East France. Central European Journal of Geosciences 4, 357-375.

Winograd, I.J., Landwehr, J.M., Ludwig, K.R., Coplen, T.B., Riggs, A.C., 1997. Duration and structure of the past four interglaciations. Quaternary Research 48, 141-154.

Wolkowinsky, A. J., Granger, D. E., 2004. Early Pleistocene incision of the San Juan River, Utah, dated with ^{26}Al and ^{10}Be, Geology 32, 749-752.

Figures captions:

Fig. 1. A) Geological map of the study area (after Colomb and Roux, 1978; Molliex et al., 2011). SCF is the Salon-Cavaillon fault. B) Regional morphodynamic context. The black frame correspond to the extent of the Fig. 1A.

Fig. 2. Schematic 3D block diagram showing the relative chronology of the Quaternary deposits associated to the downstream part of the Durance River before and after its last diversion.

Fig. 3. Field photographs of the sampled sections. A) Miramas terrace. B) Luquier terrace. See Fig. 1 for locations.

Fig. 4. Schematic diagrams showing the effect of denudation processes on surface cosmogenic concentrations. A: terrace with homogeneous lithology. B: terrace with heterogeneous lithology).

Fig. 5. Exposure age and denudation rate scenario for the Miramas terrace. A) Graphic representation of the in-situ produced ^{10}Be decrease in the Miramas terrace and the best-fit curve of the exposure age/denudation rate combination. B) χ^2 repartition as the function of denudation rate and exposure age for the Miramas terrace samples. Model uncertainties are taken as $\chi_i^2 = \chi_i^2{}_{min} + 1$, following Granger (2006).

Fig. 6. Exposure age and denudation rate scenario for the Luquier terrace. A) Graphic representation of the in-situ produced ^{10}Be decrease in the Luquier terrace and the best-fit curve of the exposure age/denudation rate combination. B) χ^2 repartition as the function of denudation rate and exposure age for the Luquier terrace samples. Uncertainties are taken as $\chi_i^2 = \chi_i^2{}_{min} + 1$, following Granger (2006).

Fig. 7. Denudation history of the alluvial terraces within the context of the glacio-eustatic cycles. The δO^{18} evolution curve is from Winograd et al. (1997).

Table caption:

Table 1. Terrestrial ^{10}Be measured in the Miramas and Luquier terraces and χ^2 minimization results. Production rate, ^{10}Be measured, ^{10}Be error and ^{10}Be theoric are in at $g(SiO_2)^{-1}$.

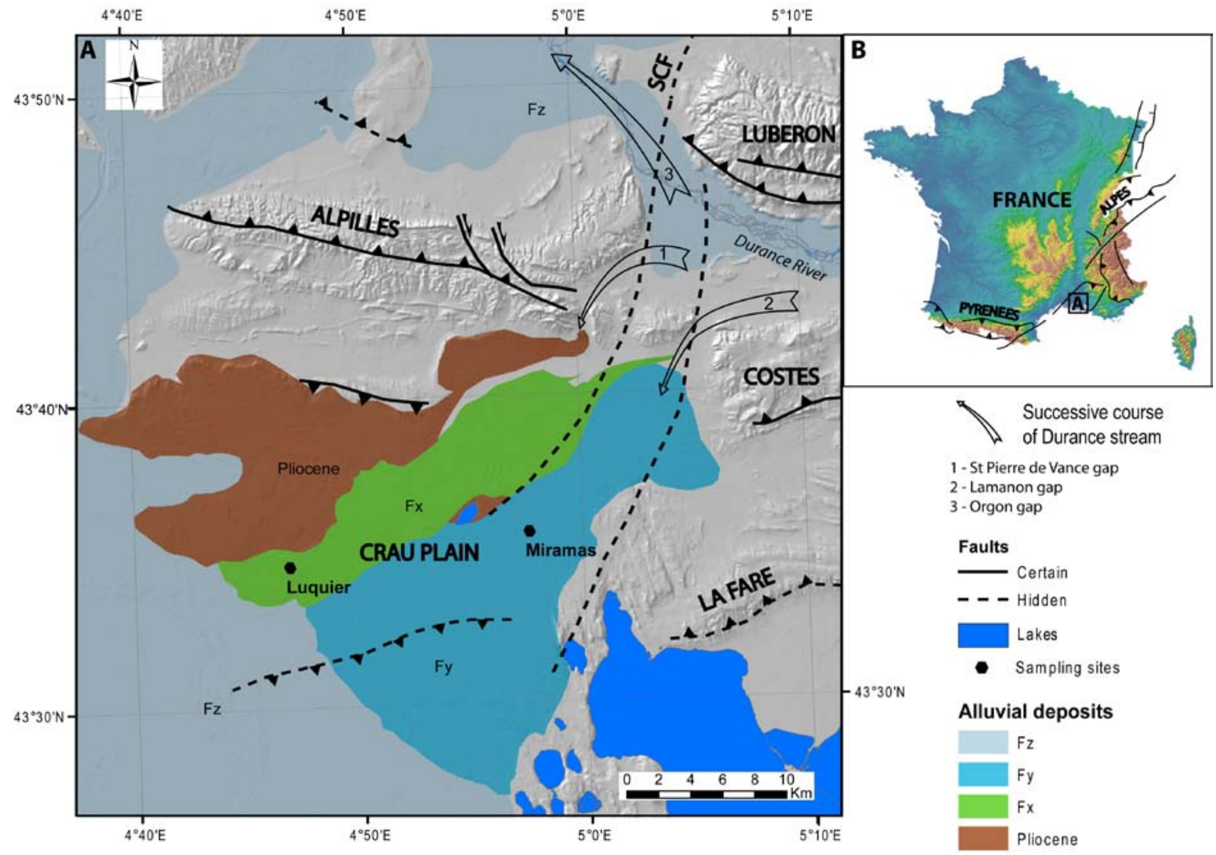

Figure1

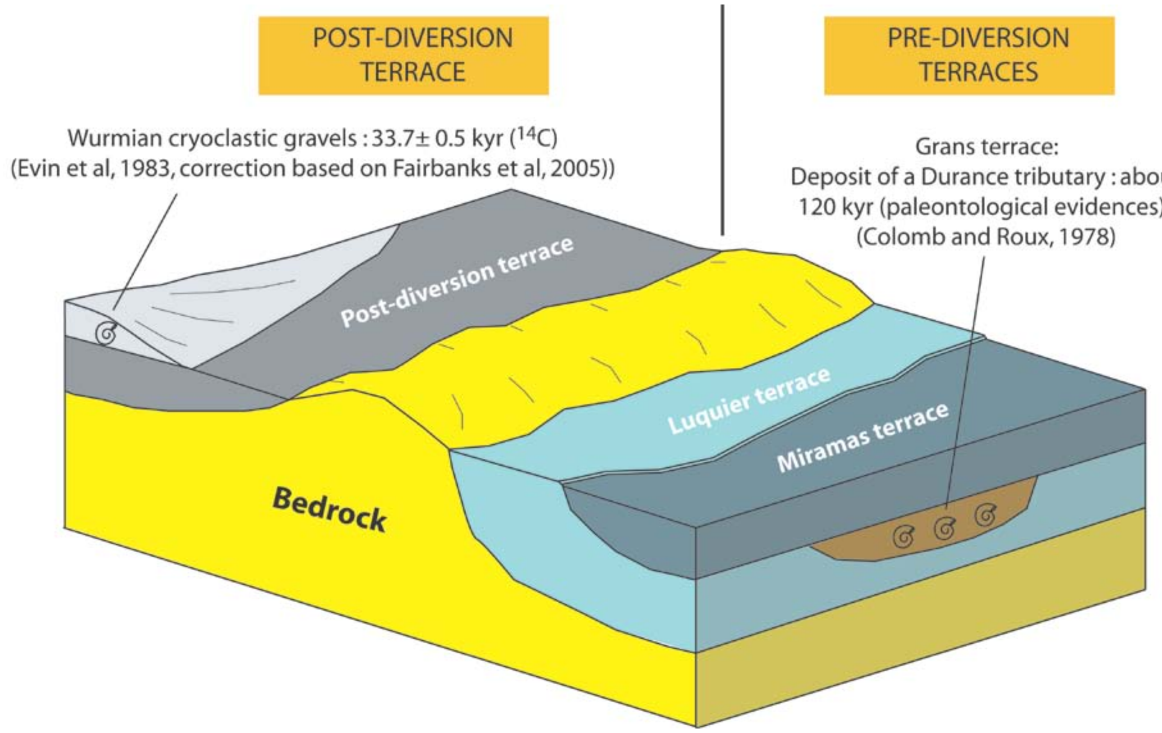
POST-DIVERSION TERRACE
PRE-DIVERSION TERRACES
Wurmian cryoclastic gravels : 33.7± 0.5 kyr (14C)
(Evin et al, 1983, correction based on Fairbanks et al, 2005))
Grans terrace:
Deposit of a Durance tributary : about 120 kyr (paleontological evidences) ;
(Colomb and Roux, 1978)
Post-diversion terrace
Luquier terrace
Miramas terrace
Bedrock

Figure 2

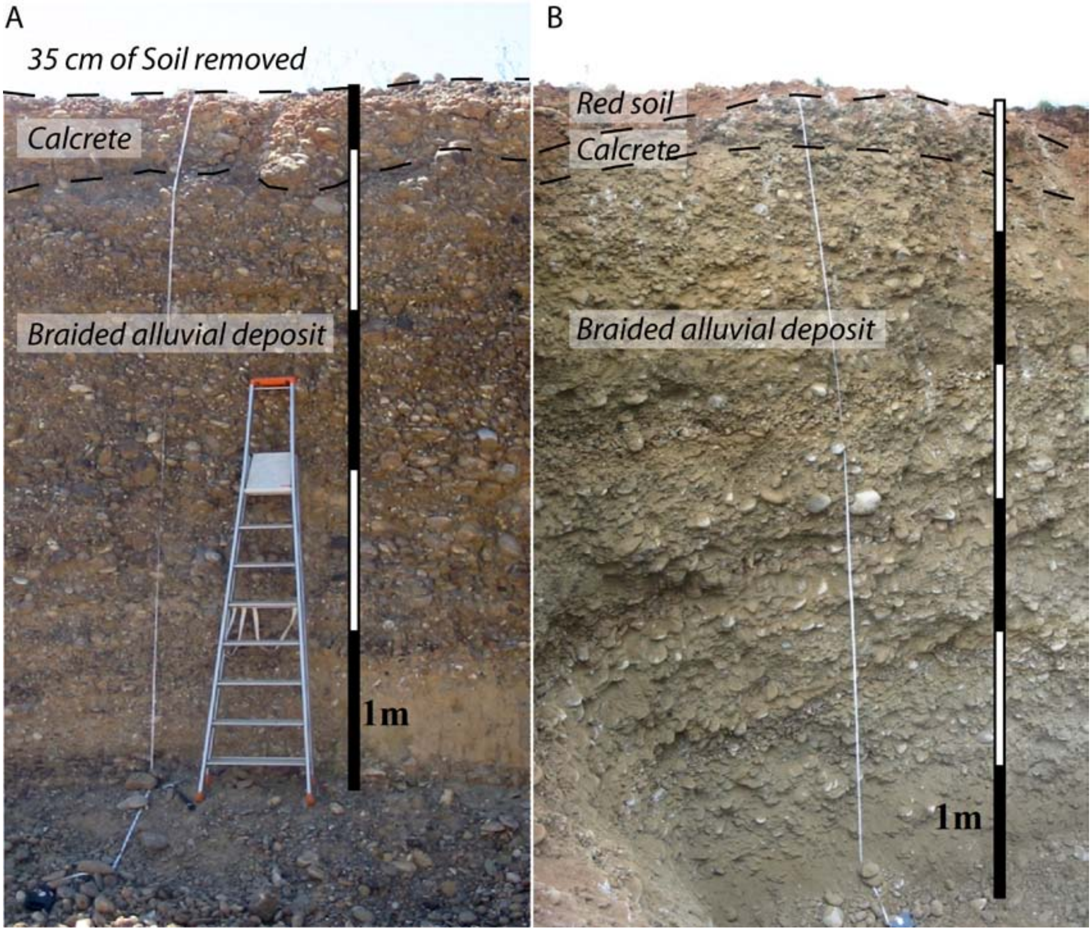
A
35 cm of Soil removed
Calcrete
Braided alluvial deposit
1m
B
Red soil
Calcrete
Braided alluvial deposit
1m

Figure 3

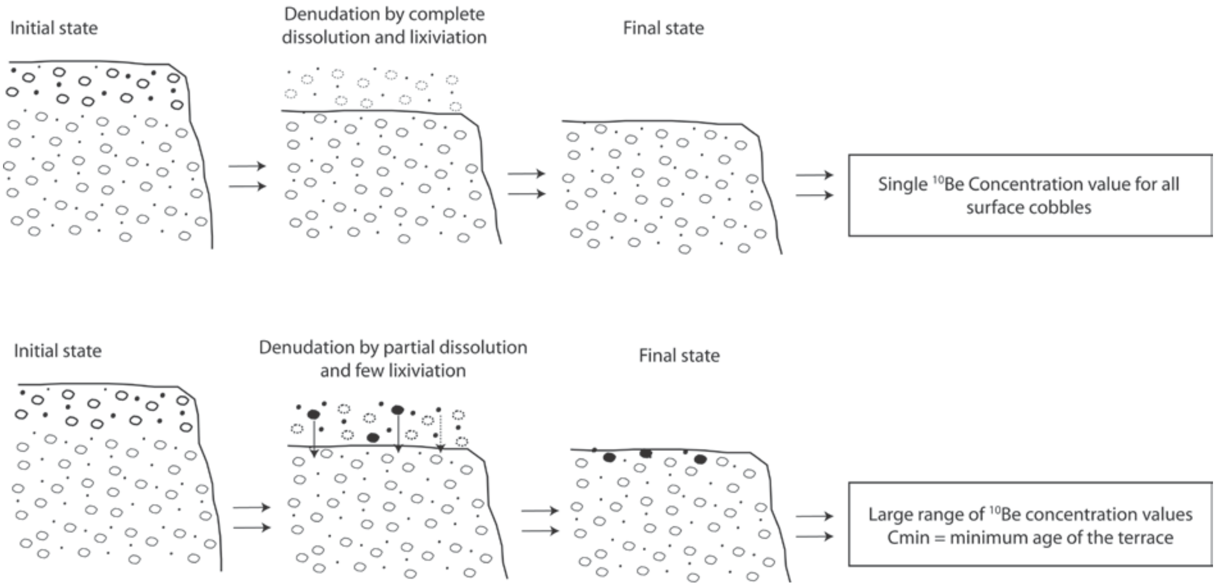
Initial state
Denudation by complete dissolution and lixiviation
Final state
Single 10Be Concentration value for all surface cobbles
Initial state
Denudation by partial dissolution and few lixiviation
Final state
Large range of 10Be concentration values
Cmin = minimum age of the terrace

Figure 4

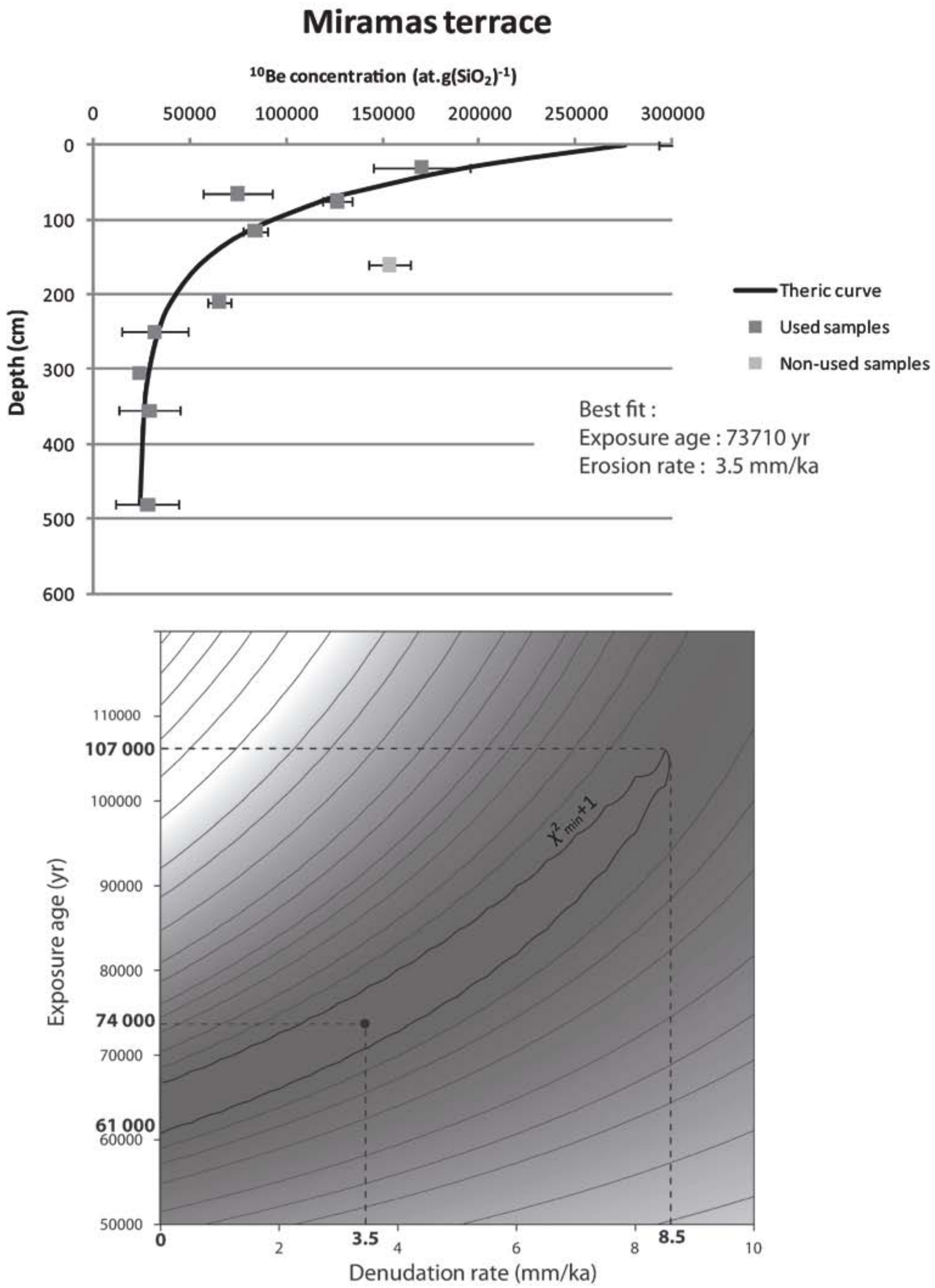
Miramas terrace
10Be concentration (at.g(SiO2)-1)
0
50000
100000
150000
200000
250000
300000
0
100
200
300
400
500
600
Depth (cm)
Theric curve
Used samples
Non-used samples
Best fit :
Exposure age : 73710 yr
Erosion rate : 3.5 mm/ka
110000
107 000
100000
90000
80000
74 000
70000
61 000
60000
50000
Exposure age (yr)
χ2 min+1
0
2
3.5
4
6
8
8.5
10
Denudation rate (mm/ka)

Figure 5

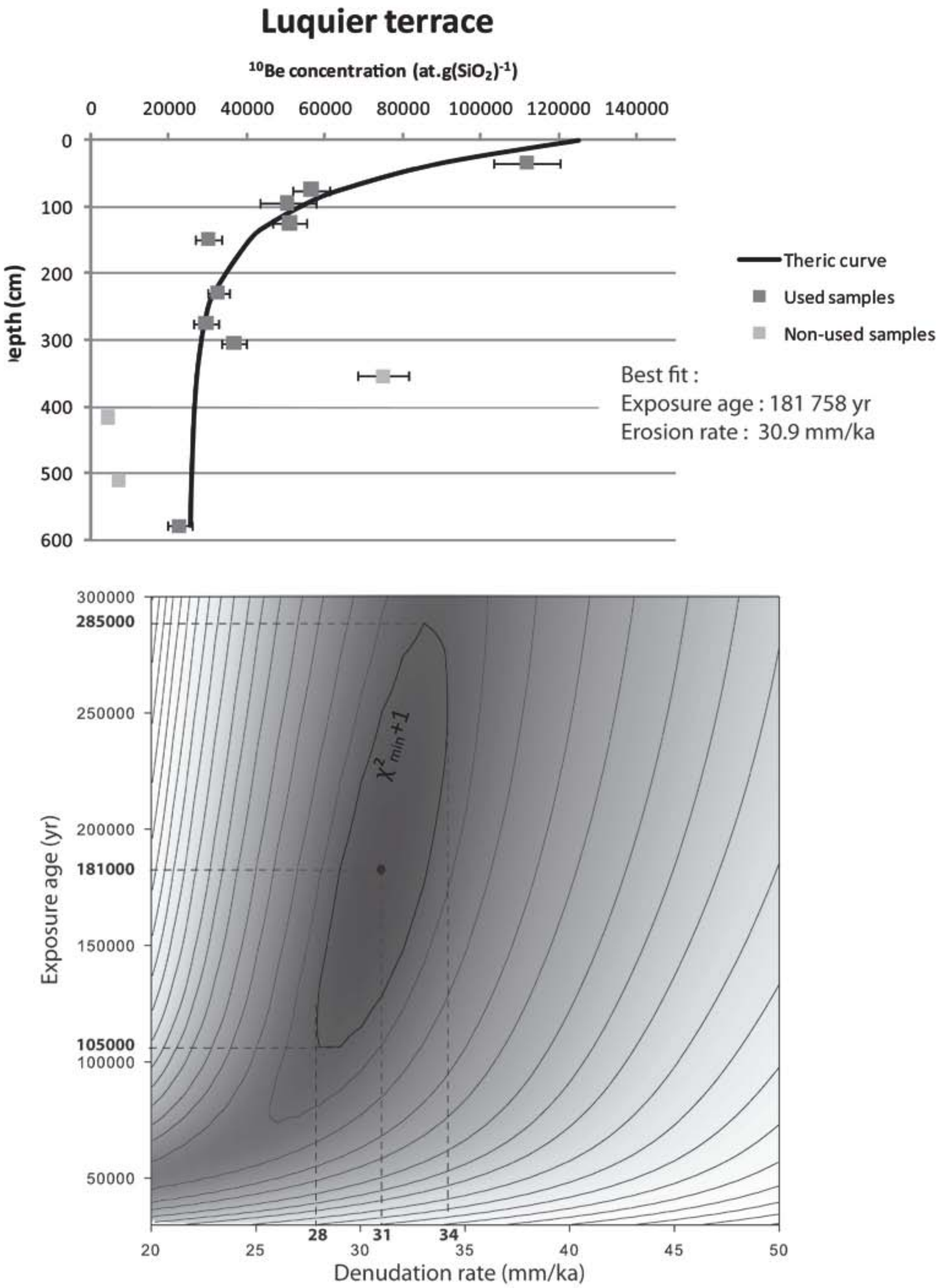
Luquier terrace
10Be concentration (at.g(SiO2)-1)
0 20000 40000 60000 80000 100000 120000 140000
Depth (cm)
0 100 200 300 400 500 600
Theric curve
Used samples
Non-used samples
Best fit :
Exposure age : 181 758 yr
Erosion rate : 30.9 mm/ka
Exposure age (yr)
300000 285000 250000 200000 181000 150000 105000 100000 50000
χ2min+1
20 25 28 30 31 34 35 40 45 50
Denudation rate (mm/ka)

Figure 6

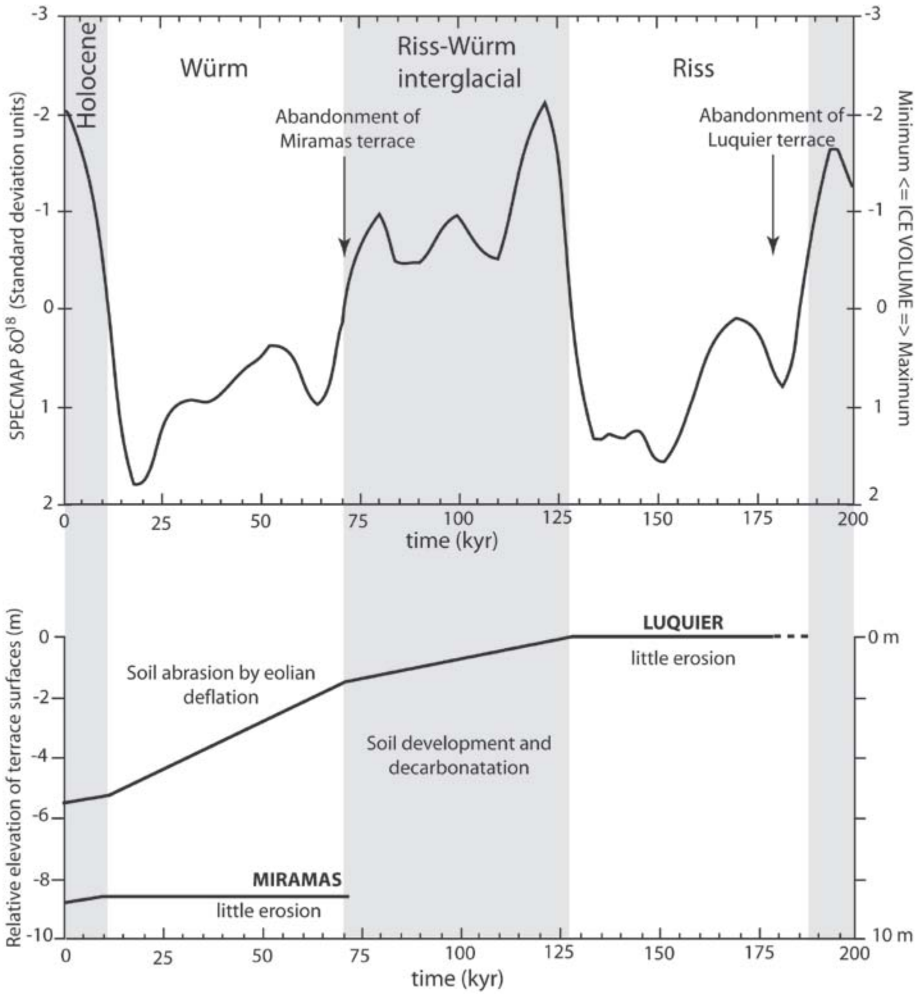

Holocene
Würm
Riss-Würm interglacial
Riss
Abandonment of Miramas terrace
Abandonment of Luquier terrace
SPECMAP δO18 (Standard deviation units)
Minimum <= ICE VOLUME => Maximum
-3
-2
-1
0
1
2
0
25
50
75
100
125
150
175
200
time (kyr)
Relative elevation of terrace surfaces (m)
0
-2
-4
-6
-8
-10
LUQUIER
little erosion
0 m
10 m
Soil abrasion by eolian deflation
Soil development and decarbonatation
MIRAMAS
little erosion
time (kyr)

Figure 7

Sample name	Longitude (°E)	Latitude (°N)	Altitude (m)	Pressure (mbar)	Depth (cm)	Production rate	[10Be] measured	[10Be] error	[10Be] theoric	χ2
MS1	4,9181	42,0618	46	1008	0	4,075	310946	18098	275229	
MS2	4,9181	42,0618	46	1008	0	4,075	493662	28538	275229	
MS3	4,9181	42,0618	46	1008	0	4,075	503523	29201	275229	
M30	4,9181	42,0618	46	1008	30	4,075	169903	25256	193689	0,8870
M65	4,9181	42,0618	46	1008	65	4,075	74449	17856	131419	10,1800
M75	4,9181	42,0618	46	1008	75	4,075	126184	7800	118277	1,0275
M115	4,9181	42,0618	46	1008	115	4,075	83588	6428	79982	0,3148
M160	4,9181	42,0618	46	1008	160	4,075	153446	10547	55202	
M210	4,9181	42,0618	46	1008	210	4,075	65087	5659	40343	19,1165
M250	4,9181	42,0618	46	1008	250	4,075	31633	17136	33764	0,0155
M305	4,9181	42,0618	46	1008	305	4,075	23613	2479	28816	4,4057
M355	4,9181	42,0618	46	1008	355	4,075	28785	15855	26520	0,0204
M480	4,9181	42,0618	46	1008	480	4,075	27860	16065	24382	0,0469
									Σχ2	36,0143
Sample name	Longitude (°E)	Latitude (°N)	Altitude (m)	Pressure (mbar)	Depth (cm)	Production rate	[10Be] measured	[10Be] error	[10Be] theoric	χ2
LS1	4,7907	43,5776	15	1011	0	4,006	363045	21086	125107	
LS2	4,7907	43,5776	15	1011	0	4,006	371227	21523	125107	
LS3	4,7907	43,5776	15	1011	0	4,006	431452	23832	125107	
LS4	4,7907	43,5776	15	1011	0	4,006	279202	16300	125107	
L35	4,7907	43,5776	15	1011	35	4,006	111677	8489	89016	7,1261
L75	4,7907	43,5776	15	1011	75	4,006	56492	4672	63665	2,3571
L95	4,7907	43,5776	15	1011	95	4,006	50330	7146	55160	0,4567
L125	4,7907	43,5776	15	1011	125	4,006	50868	4414	45902	1,2660
L150	4,7907	43,5776	15	1011	150	4,006	30197	3434	40503	9,0096
L230	4,7907	43,5776	15	1011	230	4,006	32557	2766	31313	0,2024
L275	4,7907	43,5776	15	1011	275	4,006	29535	3200	29007	0,0272
L305	4,7907	43,5776	15	1011	305	4,006	36701	3274	28031	7,0092
L355	4,7907	43,5776	15	1011	355	4,006	74779	6620	26986	
L415	4,7907	43,5776	15	1011	415	4,006	4447	733	26266	
L510	4,7907	43,5776	15	1011	510	4,006	7111	1058	25643	
L580	4,7907	43,5776	15	1011	580	4,006	22639	3144	25347	0,7418
									Σχ2	28,1961

Table 1